

A 3D INTENSITY MODEL BASED ON SPHERICAL HARMONICS FOR AUTOMATIC 3D SEGMENTATION OF HETEROCHROMATIN FOCI

Simon Eck¹, Karl Rohr¹, Andreas Biesdorf¹, Katharina Müller-Ott², Karsten Rippe², and Stefan Wörz¹

¹University of Heidelberg, BIOQUANT, IPMB, and DKFZ Heidelberg,
Dept. Bioinformatics and Functional Genomics, Biomedical Computer Vision Group
Im Neuenheimer Feld 267, 69120 Heidelberg, Germany

²DKFZ Heidelberg and BIOQUANT, Research Group Genome Organization & Function

ABSTRACT

We introduce a 3D model-based approach for automatic segmentation of 3D fluorescent heterochromatin foci from microscopy images. The approach employs a new 3D parametric intensity model based on a spherical harmonics (SH) expansion and can represent foci of regular and highly irregular shapes. By solving a least-squares minimization problem, the new model is directly fitted to the 3D image data, and the model parameters including the SH expansion coefficients are estimated. The approach has been successfully applied to real 3D microscopy image data and has been compared to previous approaches.

Index Terms— 3D parametric intensity model, spherical harmonics, heterochromatin, confocal light microscopy

1. INTRODUCTION

The nuclear organization of the genome consisting of euchromatin and heterochromatin is important for genome regulation and cell function. Using confocal light microscopy, high concentrations of heterochromatin or heterochromatin associated proteins can be visualized as *fluorescent foci*. Investigation of these foci under different experimental conditions provides important information about heterochromatin formation and maintenance. Since 3D microscopy images typically contain a large number of fluorescent foci, and since their size, shape, and signal intensity vary significantly (see Fig. 1), manual analysis is not feasible. Especially for foci of *irregular shape* (see the marked region in Fig. 1a for examples), manual segmentation in 3D is difficult and error-prone. Hence, automatic 3D image analysis approaches are required which can cope well with fluorescent foci of irregular shape, even in the case of high noise and intensity inhomogeneities.

Previous approaches for 3D heterochromatin segmentation often rely on global intensity thresholds (e.g., [1]). In [2], segmentation is performed by energy minimization within image regions using graph cuts. However, the aforementioned approaches do not determine an analytic representation of the foci and are limited by the resolution of the voxel grid.

In comparison, model-based approaches using *3D parametric intensity models* are not limited by the resolution of the voxel grid and allow determining an analytic representation of the foci shapes with subvoxel accuracy. Such approaches have successfully been used for 3D segmentation of subcellular structures from microscopy images (e.g., [3, 4]) and for heterochromatin analysis [5]. However, there only regularly shaped models (e.g., ellipsoids) were used.

In this work, we propose an automatic approach for 3D model-based segmentation of fluorescent foci from heterochromatin microscopy images. We introduce a new 3D parametric intensity model based on *spherical harmonics* (SH), which in comparison to [3, 4, 5] copes well with highly irregular foci shapes. SH form a complete set of basis functions defined on the sphere, enabling spherical functions to be expanded into a series of SH [6, 7]. In biomedical image analysis, SH were previously used, for example, for shape characterization (e.g., [8, 9, 10]), shape registration (e.g., [11]), and surface smoothing. However, only few approaches *directly* employ SH for model-based *segmentation* (e.g., [6, 12]). So far, such approaches were not used for microscopy images and they require training data [6] or manual initialization [12]. In our approach, training data is not necessary and the proposed 3D SH intensity model is initialized fully automatically. In addition, in contrast to previous work we use SH to formulate a parametric *intensity* model. By solving a least-squares minimization problem, the model is directly fitted to the image intensities and the model parameters including the SH expansion coefficients are estimated. These parameters provide a compact description of the shape and intensity of a 3D fluorescent focus. Our approach was applied to real 3D microscopy images and was compared to two previous approaches for segmentation of fluorescent foci.

2. METHODS

In our approach, the 3D shape of fluorescent foci is analytically described using a spherical harmonics (SH) expansion (see Section 2.1). Based on the SH expansion, we formulate a *3D SH parametric intensity model*, which represents

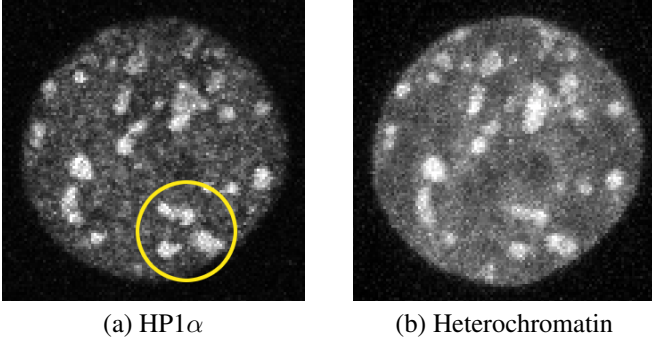


Fig. 1. Maximum intensity projections (MIPs) of a cell nucleus in a 3D two-channel microscopy image: Heterochromatin protein 1 α (HP1 α) (a) and heterochromatin (b). The circle in (a) marks an image region with three irregularly shaped HP1 α foci.

the image intensities of fluorescent foci and which considers the blurring effect of the imaging process (see Section 2.2). To automatically segment 3D heterochromatin foci from microscopy images, 3D foci detection is performed and the 3D SH intensity model is directly fitted to the image intensities using least-squares minimization (see Section 2.3).

2.1. Spherical Harmonics Shape Model

We describe the 3D shape of fluorescent foci using an expansion into a series of spherical harmonics (SH) basis functions. In our application, we assume the 3D region F of a fluorescent focus to be *star-shaped*, i.e., a point $\mathbf{q} \in F$ exists such that each ray originating from \mathbf{q} intersects the surface of F exactly once. If \mathbf{q} is the origin of a spherical coordinate system, then the surface of F can be described by a 3D radius function $r(\theta, \varphi)$. Since $r(\theta, \varphi)$ is real-valued, we employ the real-valued SH basis functions [13] of *degree* l and *order* m

$$Y_l^m(\theta, \varphi) = \begin{cases} \sqrt{2}N_l^m P_l^m(\cos \theta) \cos(m\varphi) & m > 0 \\ N_l^0 P_l^0(\cos \theta) & m = 0 \\ \sqrt{2}N_l^{|m|} P_l^{|m|}(\cos \theta) \sin(|m|\varphi) & m < 0 \end{cases} \quad (1)$$

where P_l^m is an associated Legendre polynomial, and $\theta \in [0, \pi]$ and $\varphi \in [0, 2\pi)$ are the inclination and azimuth angles, respectively. The normalization coefficients $N_l^m = \sqrt{\frac{2l+1}{4\pi} \frac{(l-m)!}{(l+m)!}}$ are chosen such that the SH basis functions are orthonormal w.r.t. θ and φ [7]. Based on (1), $r(\theta, \varphi)$ can be written as the real-valued SH expansion

$$r_{SH}(\theta, \varphi) = \sum_{l=0}^{l_{max}} \left[a_l^0 N_l^0 P_l^0(\cos \theta) + \sum_{m=1}^l \left(a_l^m \cos(m\varphi) + b_l^m \sin(m\varphi) \right) \cdot \sqrt{2} N_l^m P_l^m(\cos \theta) \right] \quad (2)$$

with the *series degree* l_{max} and the expansion coefficients $\mathbf{a} = (a_0^0, \dots, a_{l_{max}}^0)^T$ and $\mathbf{b} = (b_1^1, \dots, b_{l_{max}}^1)^T$, i.e., the weights of the SH basis functions. With increasing value of l_{max} , the

number of the SH basis functions also increases and more complex shapes can be described. For $l_{max} = 0$, the shape is equivalent to a sphere with radius a_0^0 .

2.2. 3D Parametric Intensity Model

The real-valued SH expansion in (2) describes the shape of a star-shaped 3D object, such as a fluorescent focus. Based on (2), we can formulate an ideal step-shaped 3D intensity model

$$g_{SH,ideal}(\mathbf{x}) = \begin{cases} 1 & 0 \leq r \leq r_{SH}(\theta, \varphi) \\ 0 & otherwise \end{cases} \quad (3)$$

where $\mathbf{x} = (x, y, z)^T$ denotes the 3D position, and the spherical parameters r , θ , and φ are defined by $r(\mathbf{x}) = \sqrt{x^2 + y^2 + z^2}$, $\theta(\mathbf{x}) = \cos^{-1}\left(\frac{z}{r(\mathbf{x})}\right)$, and $\varphi(\mathbf{x}) = \tan^{-1}\left(\frac{y}{x}\right)$. To incorporate the blurring effect of the imaging process described by the point spread function (PSF) of the microscope, we incorporate a convolution of $g_{SH,ideal}(\mathbf{x})$ with a Gaussian function specified by the standard deviation σ . The 3D SH intensity model is then given by

$$g_{SH}(\mathbf{x}) = \Phi_\sigma(r + r_{SH}(\pi - \theta, \varphi + \pi)) - \Phi_\sigma(r - r_{SH}(\theta, \varphi)) \quad (4)$$

where $\Phi_\sigma(x) = \Phi\left(\frac{x}{\sigma}\right)$ is the Gaussian error function with standard deviation σ and $\Phi(x) = \int_{-\infty}^x (2\pi)^{-1/2} e^{-\xi^2/2} d\xi$. We further include a 3D rigid transform $\mathcal{R}(\mathbf{x}, \mathbf{x}_0, \boldsymbol{\alpha})$ with translation $\mathbf{x}_0 = (x_0, y_0, z_0)^T$ and rotation $\boldsymbol{\alpha} = (\alpha, \beta, \gamma)^T$ as well as background and foreground intensity levels a_0 and a_1 to obtain the final *3D SH intensity model*

$$g_{M,SH}(\mathbf{x}, \mathbf{p}) = a_0 + (a_1 - a_0)g_{SH}(\mathcal{R}(\mathbf{x}, \mathbf{x}_0, \boldsymbol{\alpha})) \quad (5)$$

where $\mathbf{p} = (\mathbf{a}, \mathbf{b}, a_0, a_1, \sigma, \boldsymbol{\alpha}, \mathbf{x}_0)^T$ represents the model parameters.

2.3. Automatic 3D Foci Segmentation

To automatically segment 3D heterochromatin foci from microscopy images, we propose a two-step approach consisting of *3D foci detection* and *3D model-fitting* of the 3D SH intensity model. In the first step, we apply a 3D Gaussian filter to denoise the image and discard all intensity values below a clipping threshold to suppress the image background. We then perform a local maxima search within cubic 3D regions-of-interest (ROIs) to detect 3D foci. The optimal clipping threshold for each cell nucleus is automatically computed based on the 3D intensity histogram h_i of the i -th nucleus by $T_{clip} = \mu_i + c \cdot \sigma_i$, where μ_i and σ_i denote the mean and standard deviation of h_i , and c is a constant parameter (e.g., $c = 2$). c is determined once for a biological experiment and remains unchanged for all images. To compute h_i , 3D segmentation of the nuclei is performed by 3D Gaussian filtering and 3D Otsu thresholding.

In the second step, to determine the model parameters \mathbf{p} , the 3D SH intensity model $g_{M,SH}(\mathbf{x}, \mathbf{p})$ in (5) is fitted to the

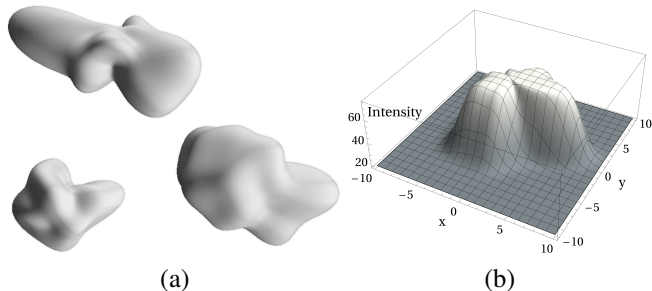


Fig. 2. Examples of segmented 3D SH intensity models from the real 3D microscopy image in Fig. 1a (see the marked region). (a) 3D visualization of the foci shapes (b) 3D plot of the 2D intensity profile of a cross-section ($z = 0$) of the focus at the right of (a).

image intensities $g(\mathbf{x})$ within spherical ROIs by using a least-squares minimization of the objective function

$$\sum_{\mathbf{x} \in ROI} (g_{M,SH}(\mathbf{x}, \mathbf{p}) - g(\mathbf{x}))^2 \rightarrow \min.$$

For the minimization we use the method of Levenberg and Marquardt which incorporates first order partial derivatives of $g_{M,SH}$ w.r.t. the model parameters \mathbf{p} . All partial derivatives are derived analytically. The minimization is performed for each detected 3D focus from the first step and the position is used to initialize the translation parameters \mathbf{x}_0 of $g_{M,SH}$.

3. EXPERIMENTAL RESULTS

We have applied our approach to 33 real 3D two-channel microscopy images of mouse fibroblast cells ($130 \times 130 \times 41$ or $250 \times 250 \times 64$ voxels). The images were acquired by a confocal laser scanning microscope. To cope with the strongly varying size of the foci (e.g., 20 – 600 voxels in one nucleus), we distinguish between small and large foci and use a series degree l_{max} of 4 and 7, respectively, in the heterochromatin protein 1 α (HP1 α) channel. For the heterochromatin (HC) channel we decrease l_{max} by one since this channel exhibits a higher level of image noise and less details about the shape of the foci (see Fig. 1). As an example, Fig. 2a shows 3D segmentation results of large HP1 α foci marked in Fig. 1a. It can be seen that our model can represent highly irregular and complex shapes. Fig. 2b shows a 3D plot of the 2D intensity profile of a cross-section of the focus at the right of Fig. 2a.

For comparison, we also applied two previous approaches: An approach based on a 3D Gaussian intensity model [4] and a 3D combined approach based on region-adaptive segmentation and a 3D Gaussian intensity model [5]. Fig. 3 shows for all three approaches examples of 3D segmentation results of HP1 α foci. It can be seen that for small foci the previous approach based on a 3D Gaussian model yields relatively good results, however, it fails to accurately segment large foci of irregular shape (see the circles in Fig. 3b). The 3D combined approach generally yields a good result, however,

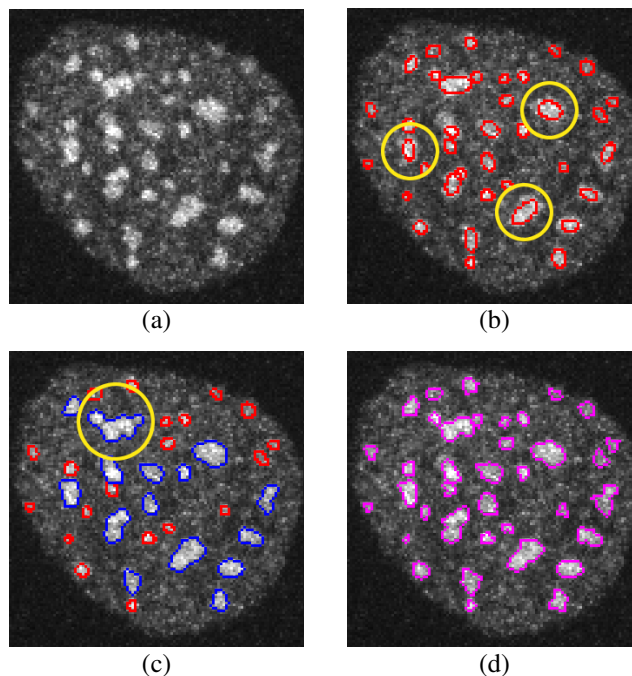


Fig. 3. MIP of (a) a cell nucleus in a 3D microscopy image and 3D segmentation results of HP1 α foci (contour overlays): (b) 3D Gaussian intensity model (red), (c) 3D combined approach based on region-adaptive segmentation (blue) and a 3D Gaussian intensity model (red), and (d) 3D SH intensity model (magenta).

for large foci of irregular shape with other foci in close proximity, undersegmentation occurs (see the circle in Fig. 3c). In comparison, the new approach yields a better result (e.g., undersegmentation does not occur) and the approach can cope well with foci of different sizes and highly irregular shapes (see Fig. 3d).

To quantify the segmentation accuracy, we computed the Dice coefficient between the 3D segmentation results and 3D ground truth data. Ground truth was provided manually by an expert E_1 for 3D foci in seven 3D microscopy images (75 foci in total, 45 HP1 α foci and 30 HC foci). To determine the interobserver variability, a second expert E_2 manually performed 3D segmentation. Manual 3D segmentation was performed slice-by-slice in the original microscopy images by drawing contours of the foci. For the automatic approaches, all foci were segmented using a fixed set of parameters. Note that due to the high level of image noise and a high variability of foci shapes, manual 3D segmentation of the foci is a difficult task, and therefore the interobserver variability between E_1 and E_2 was relatively high. Table 1 shows the mean value \bar{D} and the standard deviation σ_D of the Dice coefficient of the different approaches w.r.t. the ground truth provided by expert E_1 and separately for HP1 α foci and HC foci. It can be seen that the new approach outperforms the previous approaches for HP1 α and HC foci. Table 2 shows the result for all foci. In addition, we compared the automatic 3D segmen-

		Manual	3D automatic segmentation		
			Gaussian	Combined	SH
HP1 α	\bar{D}	0.700	0.662	0.699	0.707
	σ_D	0.058	0.112	0.098	0.095
HC	\bar{D}	0.685	0.635	0.654	0.726
	σ_D	0.046	0.109	0.110	0.113

Table 1. Quantitative 3D segmentation results of HP1 α and heterochromatin (HC) foci for real 3D microscopy images: Mean value \bar{D} and standard deviation σ_D of the Dice coefficient for different automatic approaches with ground truth provided by expert E_1 as well as result for manual segmentation by expert E_2 .

	Manual	3D automatic segmentation		
		Gaussian	Combined	SH
\bar{D}_{E_1}	0.694	0.651	0.682	0.714
\bar{D}_{E_2}		0.635	0.664	0.689
σ_{D,E_1}	0.054	0.111	0.105	0.102
σ_{D,E_2}		0.104	0.093	0.069

Table 2. Same as Table 1, but for all foci (HP1 α and HC) and comparison with ground truth from two experts E_1 and E_2 .

tation results w.r.t. the ground truth provided by the second expert E_2 . It can be seen that the new approach yields better results than the two previous approaches w.r.t. the ground truth results of both experts E_1 and E_2 . It also turns out that the result of the new approach is comparable to the interobserver variability (see the bold numbers in Table 2).

4. CONCLUSION

We introduced a 3D model-based approach for automatic segmentation of 3D fluorescent heterochromatin foci from microscopy images. The approach employs a new 3D parametric intensity model based on a spherical harmonics expansion for star-shaped objects and analytically describes the shapes and intensities of the foci. The approach has been successfully applied to real 3D two-channel microscopy image data and has been compared to two previous approaches. It turned out that the approach copes well with foci of highly irregular shapes and yields better results than the two previous approaches. In future, we plan to apply the approach to a larger number of 3D images to study genome regulation and cell function.

Acknowledgment. This work has been funded by the BMBF (SysTec) project EpiSys. We thank Dr. Qin Zhang (DKFZ Heidelberg, BIOQUANT, Division of Theoretical Systems Biology) for providing ground truth data.

5. REFERENCES

- [1] A.N. Ivashkevich, O.A. Martin, A.J. Smith, C.E. Redon, W.M. Bonner, R.F. Martin, and P.N. Lobachevsky, "H2AX foci as

a measure of DNA damage: A computational approach to automatic analysis," *Mutation Research*, vol. 711, no. 1-2, pp. 49–60, 2011.

- [2] O. Dzyubachyk, J. Essers, W.A. van Cappellen, C. Baldeyron, A. Inagaki, W.J. Niessen, and E. Meijering, "Automated analysis of time-lapse fluorescence microscopy images: from live cell images to intracellular foci," *Bioinformatics*, vol. 26, no. 19, pp. 2424–2430, 2010.
- [3] D. Thomann, D.R. Rines, P.K. Sorger, and G. Danuser, "Automatic fluorescent tag detection in 3D with super-resolution: application to the analysis of chromosome movement," *J. of Microscopy*, vol. 208, pp. 49–64, 2002.
- [4] S. Wörz, P. Sander, M. Pfannmöller, R.J. Rieker, S. Joos, G. Mechttersheimer, P. Boukamp, P. Lichter, and K. Rohr, "3D Geometry-Based Quantification of Colocalizations in Multi-channel 3D Microscopy Images of Human Soft Tissue Tumors," *IEEE Trans. on Medical Imaging*, vol. 29, no. 8, pp. 1474–1484, 2010.
- [5] S. Eck, K. Rohr, K. Müller-Ott, K. Rippe, and S. Wörz, "Combined Model-Based and Region-Adaptive 3D Segmentation and 3D Co-localization Analysis of Heterochromatin Foci," in *Proc. BVM'12*, Berlin, Germany, 2012, Informatik aktuell, pp. 9–14.
- [6] G. Székely, A. Kelemen, C. Brechbühler, and G. Gerig, "Segmentation of 2-D and 3-D objects from MRI volume data using constrained elastic deformations of flexible Fourier contour and surface models," *Medical Image Analysis*, vol. 1, no. 1, pp. 19–34, 1996.
- [7] G.B. Arfken, H.J. Weber, and F.E. Harris, *Mathematical Methods for Physicists*, Academic Press, sixth edition, 2005.
- [8] A. El-Baz, M. Nitzken, F. Khalifa, A. Elnakib, G. Gimel'farb, R. Falk, and M. El-Ghar, "3D Shape Analysis for Early Diagnosis of Malignant Lung Nodules," in *Proc. IPMI'11*, Kloster Irsee, Germany, 2011, vol. 6801 of *Lecture Notes in Computer Science*, pp. 772–783.
- [9] S. Singh, F. Janoos, T. Pecot, E. Caserta, K. Huang, J. Rittscher, G. Leone, and R. Machiraju, "Non-parametric Population Analysis of Cellular Phenotypes," in *Proc. MICCAI'11*, Toronto, Canada, Sept. 2011, vol. 6891 of *Lecture Notes in Computer Science*, pp. 343–351, Springer Berlin Heidelberg.
- [10] C. Ducroz, J.-C. Olivo-Marin, and A. Dufour, "Characterization of cell shape and deformation in 3D using Spherical Harmonics," in *Proc. ISBI'12*, Barcelona, Spain, 2012, pp. 848–851.
- [11] L. Shen, H.A. Firpi, A.J. Saykin, and J.D. West, "Parametric surface modeling and registration for comparison of manual and automated segmentation of the hippocampus," *Hippocampus*, vol. 19, no. 6, pp. 588–595, 2009.
- [12] M. Baust and N. Navab, "A Spherical Harmonics Shape Model for Level Set Segmentation," in *Proc. 11th European Conference on Computer Vision*. 2010, vol. 6313 of *Lecture Notes in Computer Science*, pp. 580–593, Springer Berlin Heidelberg.
- [13] R. Courant and D. Hilbert, *Methods of Mathematical Physics*, vol. II, Interscience, 1953.